nature medicine

Autocrine activation of the MET receptor tyrosine kinase in acute myeloid leukemia

Alex Kentsis[1,2], Casie Reed[1,2], Kim L Rice[3], Takaomi Sanda[1,2], Scott J Rodig[4], Eleni Tholouli[5], Amanda Christie[1,2,6], Peter J M Valk[7], Ruud Delwel[7], Vu Ngo[8], Jeffery L Kutok[4], Suzanne E Dahlberg[9], Lisa A Moreau[1,2], Richard J Byers[5,10], James G Christensen[11], George Vande Woude[12], Jonathan D Licht[3], Andrew L Kung[1,2,6], Louis M Staudt[13] & A Thomas Look[1,2]

Although the treatment of acute myeloid leukemia (AML) has improved substantially in the past three decades, more than half of all patients develop disease that is refractory to intensive chemotherapy[1,2]. Functional genomics approaches offer a means to discover specific molecules mediating the aberrant growth and survival of cancer cells[3–8]. Thus, using a loss-of-function RNA interference genomic screen, we identified the aberrant expression of hepatocyte growth factor (HGF) as a crucial element in AML pathogenesis. We found HGF expression leading to autocrine activation of its receptor tyrosine kinase, MET, in nearly half of the AML cell lines and clinical samples we studied. Genetic depletion of HGF or MET potently inhibited the growth and survival of HGF-expressing AML cells. However, leukemic cells treated with the specific MET kinase inhibitor crizotinib developed resistance resulting from compensatory upregulation of HGF expression, leading to the restoration of MET signaling. In cases of AML where MET is coactivated with other tyrosine kinases, such as fibroblast growth factor receptor 1 (FGFR1)[9], concomitant inhibition of FGFR1 and MET blocked this compensatory HGF upregulation, resulting in sustained logarithmic cell killing both *in vitro* and in xenograft models *in vivo*. Our results show a widespread dependence of AML cells on autocrine activation of MET, as well as the key role of compensatory upregulation of HGF expression in maintaining leukemogenic signaling by this receptor. We anticipate that these findings will lead to the design of additional strategies to block adaptive cellular responses that drive compensatory ligand expression as an essential component of the targeted inhibition of oncogenic receptors in human cancers.

We used a doxycycline-inducible retroviral RNAi library of 5,087 barcoded shRNAs targeting 1,740 human genes to screen for functional pathway dependence in OCI-AML2 cells derived from a patient with complex-karyotype AML (**Supplementary Fig. 1a**)[10]. Among the 30 genes most substantially required for the proliferation and survival of OCI-AML2 cells but not cells from a variety of nonmyeloid hematologic malignancies was HGF, the ligand of the receptor tyrosine kinase MET (**Fig. 1a**)[11]. Targeting of *HGF* and downstream mediators of the MET signaling pathway, such as *STAT3* and *MAPK1*, with two independent shRNAs markedly suppressed the growth of AML cells but not of nonmyeloid hematologic cancer cells (**Supplementary Fig. 1b–d**).

In tests of the functional consequences of HGF expression in AML cell lines, we found that in four of seven AML cell lines, but not normal $CD34^+$ cells, expressed HGF was associated with MET activation (**Fig. 1b**). Given that normal $CD34^+$ cells do not express HGF, these data indicate that HGF expression by AML cells is aberrant, whereas expression of MET is lineage appropriate. Knockdown of *HGF* using two independent specific shRNAs inhibited the growth of OCI-AML2 cells (**Fig. 1c** and **Supplementary Fig. 2a**). This effect could be rescued with recombinant HGF protein (0.1 nM) or by the transduction of complementary DNA (cDNA) encoding *HGF* (**Fig. 1c**). OCI-AML2 cell growth was also inhibited by the addition of a neutralizing antibody against HGF (100 nM) to the culture medium (**Fig. 1c**). We also showed the requirement for HGF and MET signaling in three additional AML cell lines (HEL, SKNO-1 and KG-1) by depleting *HGF* and *MET* using specific shRNAs and inhibiting MET kinase signaling using the kinase inhibitor SU11274 (1 μM) (**Supplementary Figs. 3–5**). Inhibition of HGF and MET signaling led to a significant increase in the apoptosis of HGF-expressing cells (**Fig. 1d**) without

[1]Department of Pediatric Oncology, Dana-Farber Cancer Institute, Harvard Medical School, Boston, Massachusetts, USA. [2]Division of Hematology and Oncology, Children's Hospital Boston, Harvard Medical School, Boston, Massachusetts, USA. [3]Division of Hematology and Oncology, Northwestern University Feinberg School of Medicine, Chicago, Illinois, USA. [4]Department of Pathology, Brigham and Women's Hospital, Harvard Medical School, Boston, Massachusetts, USA. [5]Department of Haematology, Manchester Royal Infirmary, Central Manchester University Hospitals National Health Service Foundation Trust, and Manchester Academic Health Science Centre, Manchester, UK. [6]Lurie Family Imaging Center, Dana-Farber Cancer Institute, Boston, Massachusetts, USA. [7]Department of Hematology, Erasmus Medical Center, Rotterdam, The Netherlands. [8]Division of Hematopoietic Stem Cell and Leukemia Research, City of Hope National Medical Center, Duarte, California, USA. [9]Department of Biostatistics and Computational Biology, Dana-Farber Cancer Institute, Boston, Massachusetts, USA. [10]School of Cancer and Enabling Sciences, Faculty of Medical and Human Sciences, University of Manchester, Manchester, UK. [11]Department of Research Pharmacology, Pfizer Global Research and Development, La Jolla, California, USA. [12]Department of Molecular Oncology, Van Andel Research Institute, Grand Rapids, Michigan, USA. [13]Center for Cancer Research, National Cancer Institute, National Institutes of Health, Bethesda, Maryland, USA. Correspondence should be addressed to A.T.L. (thomas_look@dfci.harvard.edu).

Received 30 March 2011; accepted 30 April 2012; published online 10 June 2012; doi:10.1038/nm.2819

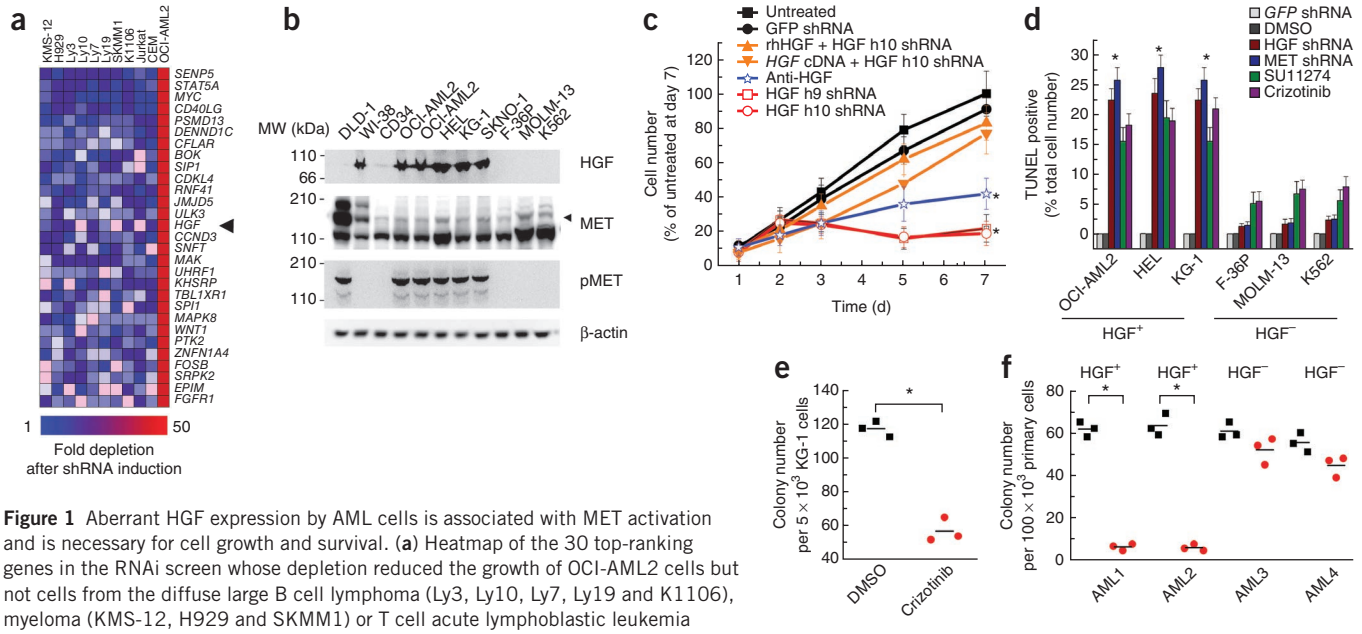

Figure 1 Aberrant HGF expression by AML cells is associated with MET activation and is necessary for cell growth and survival. (**a**) Heatmap of the 30 top-ranking genes in the RNAi screen whose depletion reduced the growth of OCI-AML2 cells but not cells from the diffuse large B cell lymphoma (Ly3, Ly10, Ly7, Ly19 and K1106), myeloma (KMS-12, H929 and SKMM1) or T cell acute lymphoblastic leukemia (Jurkat and CEM) lines. The relative cell depletion is indicated with a blue-to-red color gradient. The master myeloid transcription factor *SPI1* served as the internal positive control; *HGF* is indicated with an arrowhead. (**b**) Western blot analysis of lysates from colon carcinoma DLD-1 cells with *MET* amplification, WI-38 fibroblasts expressing HGF, normal human CD34$^+$ cells and seven AML cell lines; OCI-AML2 is duplicated. HGF is detected with an apparent mobility of 90 kDa, corresponding to its intracellular pro form, whereas MET is detected as both pro and mature forms in DLD-1 cells (180 and 140 kDa, respectively) and predominantly as the mature form (140 kDa) in AML cells (arrowhead). pMET, phosphorylated MET. (**c**) The growth of OCI-AML2 cells is inhibited by the transduction of specific shRNAs targeting HGF (h9 and h10) or by treatment with a neutralizing antibody to HGF (anti-HGF) but not by transduction of control shRNA (GFP) or by concomitant rescue with *HGF* cDNA or recombinant human HGF (rhHGF). Measurements are normalized to the value for untreated cells at day 7 and are shown as means and s.d. of three biological replicates. *$P < 0.05$ compared to untreated control by *t* test. (**d**) TUNEL analysis of AML cells that express HGF and activate MET (OCI-AML2, HEL and KG-1) compared to those that lack HGF expression (F-36P, MOLM-13 and K562) as a function of depletion of HGF or MET using RNAi, treatment with the MET kinase inhibitor SU11274 or crizotinib for 48 h. Transduction with *GFP* shRNA and treatment with DMSO served as controls. Values are means and s.d. of three biological replicates. *$P < 0.05$ compared to DMSO or *GFP* shRNA control by *t* test. (**e**,**f**) Methylcellulose colony-forming assays of KG-1 cells (**e**) in the presence of DMSO control (black box) or crizotinib (red circle), and primary AML specimens (**f**) with aberrant HGF expression (AML1 and AML2) compared to those lacking HGF (AML3 and AML4). Individual data points and means (bars) of three biological replicates are shown. *$P < 0.05$ compared to DMSO control by *t* test.

the induction of cell-cycle arrest (**Supplementary Fig. 3**). In addition, treatment with the specific MET kinase inhibitor crizotinib (100 nM) led to decreased colony formation of HGF-expressing primary AML samples (**Fig. 1e**,**f**). Taken together, our findings indicate that cell-autonomous production of HGF causes autocrine activation of MET and is necessary for the proliferation or survival of HGF-expressing AML cells.

To estimate the prevalence of aberrant HGF and MET signaling in patients with AML, we used immunohistochemistry to detect the coexpression of HGF and MET in bone marrow biopsy specimens from 138 adults with a broad spectrum of AML subtypes (**Fig. 2a–c** and **Supplementary Fig. 6a–e**). These proteins were expressed together in 58 (42%) of the patients (**Fig. 2c**), often in association with specific genetic abnormalities, including the *PML-RARA* and *AML1-ETO* (also known as *RUNX1-RUNX1T1*) translocations (**Supplementary Fig. 6f**). Using a capillary isoelectric focusing electrophoresis nano-immunoassay, which allows for precise quantification of differences in protein expression and phosphorylation, we observed expression of HGF and activation of MET in 5 (38%) of 13 viably frozen bone marrow aspirate specimens (**Supplementary Fig. 7**) and confirmed these results using flow cytometry (**Supplementary Fig. 8**). In the cohort we examined, there was no statistically significant difference in survival between patients with and without aberrant HGF expression (**Supplementary Fig. 6g**). An additional analysis of the gene expression profiles of primary blasts from 285 patients with AML using unsupervised clustering also revealed the high expression of HGF in a subset of patients with AML[12], including patients with the with *PML-RARA* or *AML1-ETO* translocations (**Supplementary Fig. 9**).

Because HGF expression is associated with specific biologic subtypes of AML, we hypothesized that it might be induced by chimeric transcription factors that act in *trans* on the *HGF* locus to drive AML pathogenesis. Consistent with this concept, we did not detect any copy number changes (**Supplementary Fig. 10a**,**b**), mutations of the *HGF* promoter (**Supplementary Fig. 10c**) or allelic skewing of single nucleotide polymorphism expression (**Supplementary Fig. 10d**) in human AML cell lines with aberrant HGF expression. To test this predicted *trans*-acting mechanism directly, we transduced primary lineage-depleted mouse hematopoietic cells with fusion-protein–encoding retroviruses and monitored them for expression of HGF and activation of MET using nanoimmunoassays. Cells transduced with retroviruses encoding *PML-RARA*, *PLZF-RARA* (also known as *ZBTB16-RARA*) or *AML1-ETO* expressed HGF (**Fig. 2d** and **Supplementary Fig. 11**) and showed phosphorylation of MET (**Fig. 2e** and **Supplementary Fig. 11**). The transformed cells were sensitive to MET kinase inhibition in serial replating colony-formation assays (**Fig. 2f** and **Supplementary Fig. 11**) and showed downregulation of MET phosphorylation (**Fig. 2g** and **Supplementary Fig. 11**). Thus, distinct chimeric transcription factors can induce expression of HGF, leading to aberrant MET activation and functional dependence on HGF and MET signaling.

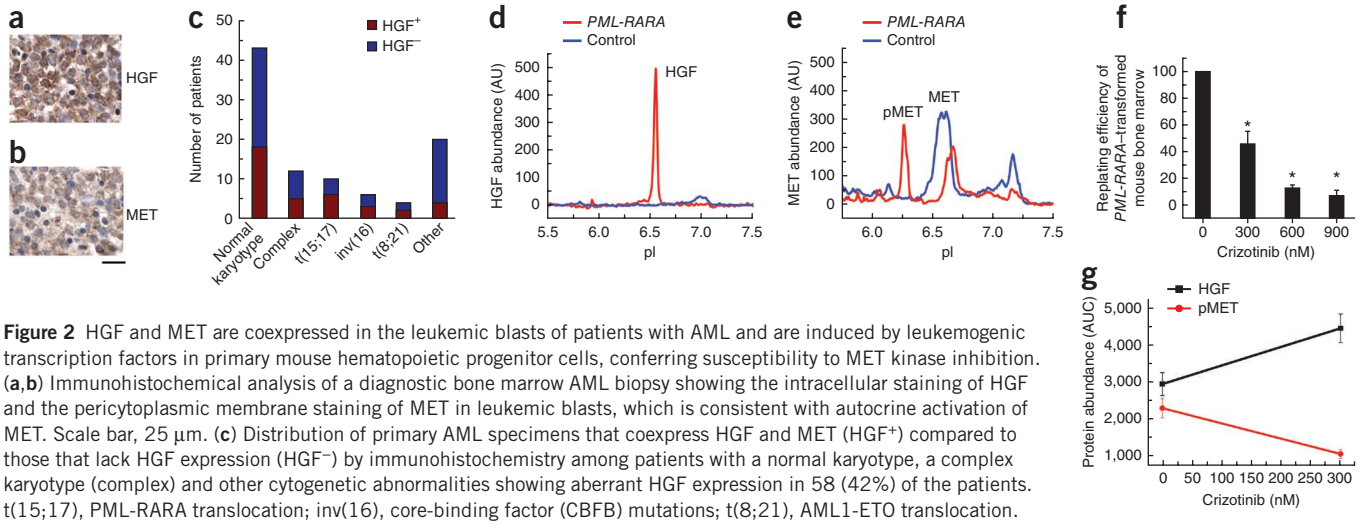

Figure 2 HGF and MET are coexpressed in the leukemic blasts of patients with AML and are induced by leukemogenic transcription factors in primary mouse hematopoietic progenitor cells, conferring susceptibility to MET kinase inhibition. (**a**,**b**) Immunohistochemical analysis of a diagnostic bone marrow AML biopsy showing the intracellular staining of HGF and the pericytoplasmic membrane staining of MET in leukemic blasts, which is consistent with autocrine activation of MET. Scale bar, 25 µm. (**c**) Distribution of primary AML specimens that coexpress HGF and MET (HGF^+) compared to those that lack HGF expression (HGF^-) by immunohistochemistry among patients with a normal karyotype, a complex karyotype (complex) and other cytogenetic abnormalities showing aberrant HGF expression in 58 (42%) of the patients. t(15;17), PML-RARA translocation; inv(16), core-binding factor (CBFB) mutations; t(8;21), AML1-ETO translocation. (**d**) Abundance of mouse HGF at 7 d after retroviral transduction of mouse hematopoietic progenitors with *PML-RARA* (red) or vector control (blue) showing induction of HGF expression as measured with nanoimmunoassays. AU, arbitrary units (**d**,**e**). (**e**) Abundance of MET and pMET 7 d after retroviral transduction of mouse hematopoietic progenitors with *PML-RARA* (red) or vector control (blue) showing activation of MET after induction of HGF expression. Equal protein loading was confirmed by the use of β_2-microglobulin as the loading control. (**f**) The colony replating efficiency of *PML-RARA*–transformed mouse hematopoietic progenitor cells as a function of increasing concentrations of crizotinib. Values are normalized to the number of colonies in mock-treated cells and plotted as means and s.d. of three biological replicates. $^*P < 0.05$ compared to DMSO-treated cells. AUC, area under the curve. (**g**) Abundance of HGF (black) and pMET (red) in *PML-RARA*–transformed mouse hematopoietic progenitor cells treated with varying concentrations of crizotinib showing inhibition of MET phosphorylation and upregulation of HGF.

To assess the potential of HGF and MET signaling as a therapeutic target, we investigated the sensitivity of HGF- and MET-dependent AML cell lines to chemical inhibition of the MET kinase using the specific MET and anaplastic lymphoma receptor tyrosine kinase (ALK) inhibitor crizotinib[13], which permits targeting of MET in AML because ALK is not expressed by hematopoietic cells or by any of the AML cell lines studied to date (**Supplementary Fig. 3b**). The growth of AML cell lines with aberrant HGF expression and MET activation was strongly inhibited by treatment with crizotinib (100 nM), whereas the growth of cell lines lacking HGF expression and MET activation was unaffected by crizotinib treatment (**Fig. 1d** and **Supplementary Fig. 4e**,**f**). However, HGF-expressing cells treated for more than 6 d with crizotinib seemed to regain their normal growth rate (**Fig. 3a** and **Supplementary Fig. 12a**,**b**).

Further experiments to determine the origin of the acquired resistance to crizotinib using quantitative nanoimmunoassays showed a profound inhibition of MET activation within 12 h of crizotinib treatment in OCI-AML2 cells (**Supplementary Fig. 13a**) that was associated with the induction of apoptosis (**Supplementary Fig. 14**). In addition, we observed a 13-fold upregulation of HGF in crizotinib-treated compared to vehicle-treated OCI-AML2 cells (**Supplementary Fig. 13b**), which occurred in concert with the recovery of the amount of phosphorylated MET after 10 d of treatment (**Supplementary Fig. 13a**), accounting for the restoration of pretreatment cell growth rates (**Fig. 3a**). This finding, confirmed in three different AML cell lines (**Supplementary Fig. 12c**), reflects an increased biallelic expression of *HGF* mRNA after crizotinib treatment (**Supplementary Fig. 15**). The recovery of MET phosphorylation corresponded with a recovery in the abundance of phosphorylated CRKL, phosphorylated signal transducer and activator of transcription 3 (STAT3) and phosphorylated mitogen-activated protein kinases 3/1 (ERK1/2) (**Supplementary Fig. 13d–f**), which are all associated with marked upregulation of HGF (**Supplementary Fig. 13b**). Depletion of HGF with a specific shRNA partially mitigated the compensatory upregulation of HGF in response to MET kinase inhibition, but this strategy was only partially successful in inhibiting leukemia growth *in vivo* because of the intrinsic variability in knockdown efficiency (**Supplementary Figs. 16** and **17**). Although the rapid development of crizotinib resistance was somewhat surprising to us, the selective pressure to maintain MET phosphorylation by upregulation of HGF reinforces our original conclusion that specific types of AML require aberrant HGF-mediated activation of MET signaling for sustained growth and survival.

As activation of MET can occur in AMLs that also harbor aberrant activation of other receptor tyrosine kinases, we reasoned that the combined inhibition of the signaling pathways that are coactivated with MET might be required to block the compensatory upregulation of HGF. In this study, we focused on the coactivation of FGFR1 with HGF and MET in KG-1 cells, which bear a *FGFR1OP2-FGFR1* chromosomal translocation and are derived from aggressive 8p11 myeloproliferative syndrome/stem cell leukemia[9]. After treating KG-1 cells with various concentrations of crizotinib and PD173074, a specific and potent inhibitor of the FGFR1 tyrosine kinase[14], we analyzed the effects using an isobologram analysis (**Supplementary Fig. 18a**). Nearly all dose combinations of PD173074 and crizotinib produced synergistic effects, as indicated by their low combination index values (**Supplementary Fig. 18a**). We found that the effect of PD173074 (20 nM) was mediated specifically by inhibition of FGFR1, as depletion of FGFR1 sensitized KG-1 cells to treatment with crizotinib (**Supplementary Fig. 19**).

Combination treatment of KG-1 cells with 100 nM crizotinib and 20 nM PD173074 (corresponding to their individual half-maximal inhibitory concentration (IC_{50}) values) prevented the compensatory upregulation of HGF (**Fig. 3b**), leading to sustained inhibition of MET phosphorylation (**Fig. 3c**) and sustained blockade of downstream signaling pathways (**Supplementary Fig. 18b–f**). This strategy also led to potent induction of apoptosis and logarithmic cell killing that was sustained for 14 d of treatment (**Fig. 3**). We confirmed the on-target effect of PD173074 by specifically depleting cells of FGFR1 by

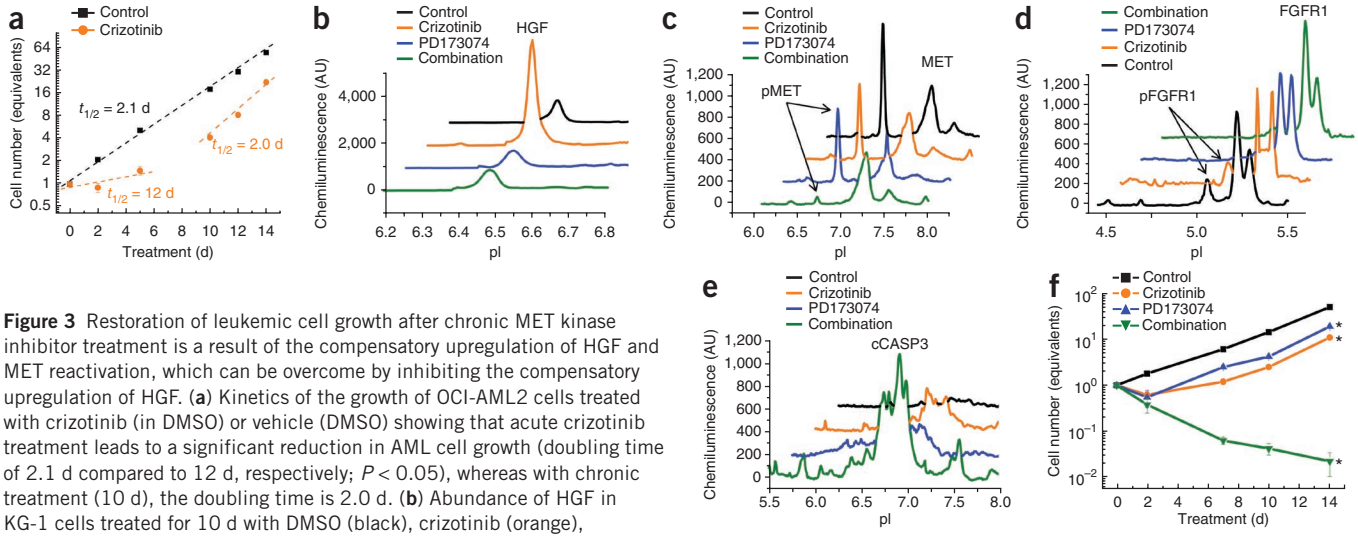

Figure 3 Restoration of leukemic cell growth after chronic MET kinase inhibitor treatment is a result of the compensatory upregulation of HGF and MET reactivation, which can be overcome by inhibiting the compensatory upregulation of HGF. (**a**) Kinetics of the growth of OCI-AML2 cells treated with crizotinib (in DMSO) or vehicle (DMSO) showing that acute crizotinib treatment leads to a significant reduction in AML cell growth (doubling time of 2.1 d compared to 12 d, respectively; $P < 0.05$), whereas with chronic treatment (10 d), the doubling time is 2.0 d. (**b**) Abundance of HGF in KG-1 cells treated for 10 d with DMSO (black), crizotinib (orange), PD173074 (blue) or a combination of crizotinib and PD173074 (green) as measured by quantitative nanoimmunoassay with β_2-microglobulin as the loading control (**Supplementary Fig. 16e**). (**c**) MET activation as assessed by the abundance of pMET in KG-1 cells treated for 10 d with the indicated drugs showing the maintenance of MET signaling in cells treated with crizotinib or PD173074 but not in cells exposed to the combination treatment. (**d**) FGFR1 activation as assessed by the abundance of phosphorylated FGFR1 (pFGFR1) in KG-1 cells treated for 10 d with the indicated drugs showing a lack of an effect of crizotinib on FGFR1 activity. (**e**) Induction of apoptosis as assessed by the abundance of cleaved caspase 3 (cCASP3) in KG-1 cells treated for 10 d showing substantially greater induction of apoptosis in cells treated with a combination of crizotinib and PD173074 compared to treatment with either drug alone. (**f**) Combined treatment of KG-1 cells with crizotinib and PD173074 leads to sustained logarithmic cell killing compared to treatment with either drug alone. Values are means and s.d. of three biological replicates. $^*P < 0.05$ compared to either drug alone by *t* test. AU, arbitrary units.

shRNA knockdown and showing that cells depleted of FGFR1, but not those transduced with the vector control, fail to upregulate HGF in response to chronic (≥10 d) crizotinib treatment (**Supplementary Fig. 19c**). Thus, FGFR1 activity is required for the compensatory upregulation of HGF in response to MET inhibition.

We then evaluated the simultaneous inhibition of MET and a blockade of compensatory HGF expression in KG-1 cells modified to express luciferase for bioluminescence imaging, which we engrafted into immunocompromised mice by tail vein injection. We treated the leukemic mice with vehicle control, crizotinib (50 mg per kg body weight) alone, PD173074 (25 mg per kg body weight) alone or a combination of the two agents by daily oral gavage 10 d after transplantation of the leukemia cells. Mice treated with the single drugs or the vehicle control continued to show exponentially growing leukemia, whereas mice treated with both crizotinib and PD173074 had significant regression in disease after 10 d of therapy, as measured by bioluminescence (**Fig. 4a**,**b**). We confirmed these results by flow cytometry, finding a near-complete ablation of $CD45^+$ human cells in the peripheral blood and bone marrow of mice treated with the combination of crizotinib and PD173074 but not in those treated with either drug alone or with the vehicle control (**Fig. 4c**,**d**). Although PD173074 alone had more potent effects on cell growth

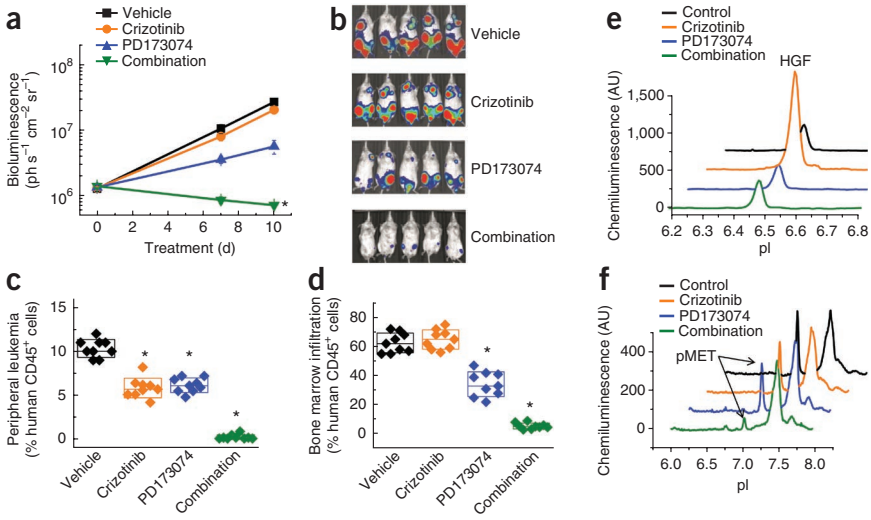

Figure 4 Combined inhibition of MET and FGFR1 blocks the compensatory upregulation of HGF, leading to sustained inhibition of MET in KG-1 cells and near-complete regression of AML *in vivo*. (**a**) Bioluminescence measurements of leukemic mice engrafted with luciferase-modified KG-1 cells and treated with vehicle control (black), crizotinib alone (orange), PD173074 alone (blue) or a combination of crizotinib and PD173074 (green) by daily oral gavage. Values are means and s.d. of each treatment group ($n = 9$ mice per group). $^*P < 0.05$ compared to all three other groups. (**b**) Bioluminescent photographs of representative mice from each treatment group (the blue-to-red color gradient indicates increasing bioluminescence intensities). (**c**,**d**) Scatter plots of the fraction of human $CD45^+$ KG-1 cells in the peripheral blood (**c**) and bone marrow (**d**) of mice after 10 d of treatment showing near-complete elimination of human AML cells in mice treated with the combination of crizotinib and PD173074. Boxes denote means and s.d. for each group ($n = 9$ mice per group). $^*P < 0.05$ compared to the vehicle-treated control group by *t* test. (**e**,**f**) Abundance of HGF (**e**) and pMET (**f**) in human CD45-selected KG-1 cells isolated from the bone marrow of mice after 10 d of treatment, as indicated, showing blockade of compensatory HGF upregulation in response to crizotinib treatment by the combined inhibition of MET and FGFR1 and the sustained inhibition of MET activation. AU, arbitrary units

than crizotinib alone, they were only modest at best, indicating that the striking therapeutic synergy of this combination stems primarily from the PD173074-induced blockade of compensatory HGF upregulation in response to crizotinib treatment (**Fig. 4e**,**f**).

We have identified aberrant HGF and MET signaling as a requisite pathway in the growth and survival of AML cells in nearly half of the primary clinical samples from a large group. In addition to *HGF*, our genome-wide shRNA screen identified a number of other genes as crucial factors in the biochemical processes that drive AML pathogenesis, which, with proper validation, could offer a functional taxonomy of AML cells, provide powerful insights into the pathophysiology of the disease and, ultimately, offer targets for improved therapy.

How does aberrant production of HGF contribute to the pathobiology of AML? We show here that dysregulated expression of this secreted growth factor, caused in part by the activity of distinct AML-associated transcription factors, leads to autocrine activation of the MET receptor and, in turn, to autocrine receptor tyrosine kinase signaling, as originally postulated on the basis of first-principle considerations[15]. Instead of direct mutational activation[16], we found that MET is activated in AML as a result of aberrant autocrine signaling by HGF, which seems to be dynamically controlled, as indicated by the upregulation of HGF in response to chronic MET kinase inhibition. Because constitutive activation of growth factor signaling pathways can have maladaptive cellular effects, such as cell-cycle arrest and senescence[17], these findings suggest that HGF deregulation and autocrine signaling provide a mechanism by which MET activity can be modulated to levels that optimize the fitness of AML cells, a property that may not be achieved by mutational activation of MET. In addition, *HGF* seems to be one of the most differentially expressed genes in the leukemia-initiating cells of AML as compared to normal hematopoietic stem cells[18], suggesting that aberrant HGF and MET signaling may contribute to the growth and survival of AML stem cells, thus strengthening the rationale for targeting this pathway.

Our study also raises the possibility that ligand-induced receptor activation may provide a general mechanism through which cancer cells can develop resistance to the therapeutic inhibition of receptor tyrosine kinase signaling. Autocrine signaling is widely prevalent in human cancers, affecting the epidermal GFR (EGFR), insulin-like GFR (IGFR), platelet-derived GFR (PDGFR), fibroblast GFR (FGFR), neurotrophic tyrosine kinase (TRK), EPH and TIE receptor families, many of which are currently being explored as therapeutic targets[19]. Indeed, ligand-dependent activation of receptor tyrosine kinases has been observed with other leukemogenic receptor tyrosine kinases, most notably the KIT oncogene and fms-related tyrosine kinase 3 (FLT3)[20]. Treatment with FLT3 kinase inhibitors leads to upregulation of the FLT3 ligand[21], which may be responsible, at least in part, for the diminished clinical efficacy of FLT3 inhibitors in patients with AML[22]. Autocrine or paracrine ligand-induced receptor activation will probably mitigate the effects of the targeted kinase inhibitors of these receptors in a manner that is analogous to the mechanisms by which HGF antagonizes inhibition of the MET kinase by crizotinib. Adaptive increases in ligand expression provide a means for cancer cell populations to re-establish the signal transduction pathways that existed before the onset of inhibitor treatment.

Clinical strategies will need to be developed to effectively overcome ligand-mediated resistance to targeted therapies. In the case of 8p11 stem cell leukemia involving *FGFR1* translocations, FGFR1 activity is required for the compensatory upregulation of HGF in response to MET inhibition. Combined inhibition of these coactivated pathways is highly synergistic as a result of the blockade of compensatory HGF upregulation, which leads to the sustained logarithmic cell killing that is required for clinically effective therapy.

METHODS

Methods and any associated references are available in the online version of the paper.

Note: Supplementary information is available in the online version of the paper.

ACKNOWLEDGMENTS

We thank A. Gutierrez, M. Mansour and E. Gjini for critical discussions and J. Gilbert for editorial advice. This research was supported by the US National Institutes of Health grant K08CA160660 (A.K.), the William Lawrence and Blanche Hughes Foundation (T.S.), the Samuel Waxman Cancer Research Foundation (J.D.L.), the V Foundation (A.T.L.) and the Intramural Research Program of the National Cancer Institute, Center for Cancer Research (L.M.S.).

AUTHOR CONTRIBUTIONS

A.K., C.R., K.L.R., T.S., A.C., E.T., V.N. and L.A.M. performed experiments. A.K., S.J.R., P.J.M.V., R.D., J.L.K., S.E.D., R.J.B., J.G.C., G.V.W., J.D.L., A.L.K., L.M.S. and A.T.L. analyzed data. A.K. and A.T.L. wrote the manuscript.

COMPETING FINANCIAL INTERESTS

The authors declare competing financial interests: details are available in the online version of the paper.

Published online at http://www.nature.com/doifinder/10.1038/nm.2819.
Reprints and permissions information is available online at http://www.nature.com/reprints/index.html.

1. Grimwade, D. *et al.* The predictive value of hierarchical cytogenetic classification in older adults with acute myeloid leukemia (AML): analysis of 1065 patients entered into the United Kingdom Medical Research Council AML11 trial. *Blood* **98**, 1312–1320 (2001).
2. Burnett, A., Wetzler, M. & Lowenberg, B. Therapeutic advances in acute myeloid leukemia. *J. Clin. Oncol.* **29**, 487–494 (2011).
3. Westbrook, T.F., Stegmeier, F. & Elledge, S.J. Dissecting cancer pathways and vulnerabilities with RNAi. *Cold Spring Harb. Symp. Quant. Biol.* **70**, 435–444 (2005).
4. Bernards, R., Brummelkamp, T.R. & Beijersbergen, R.L. shRNA libraries and their use in cancer genetics. *Nat. Methods* **3**, 701–706 (2006).
5. Ngo, V.N. *et al.* A loss-of-function RNA interference screen for molecular targets in cancer. *Nature* **441**, 106–110 (2006).
6. Whitehurst, A.W. *et al.* Synthetic lethal screen identification of chemosensitizer loci in cancer cells. *Nature* **446**, 815–819 (2007).
7. Turner, N.C. *et al.* A synthetic lethal siRNA screen identifying genes mediating sensitivity to a PARP inhibitor. *EMBO J.* **27**, 1368–1377 (2008).
8. Scholl, C. *et al.* Synthetic lethal interaction between oncogenic KRAS dependency and STK33 suppression in human cancer cells. *Cell* **137**, 821–834 (2009).
9. Gu, T.L. *et al.* Phosphotyrosine profiling identifies the KG-1 cell line as a model for the study of FGFR1 fusions in acute myeloid leukemia. *Blood* **108**, 4202–4204 (2006).
10. Wang, C., Curtis, J.E., Minden, M.D. & McCulloch, E.A. Expression of a retinoic acid receptor gene in myeloid leukemia cells. *Leukemia* **3**, 264–269 (1989).
11. Birchmeier, C., Birchmeier, W., Gherardi, E. & Vande Woude, G.F. MET, metastasis, motility, and more. *Nat. Rev. Mol. Cell Biol.* **4**, 915–925 (2003).
12. Valk, P.J. *et al.* Prognostically useful gene-expression profiles in acute myeloid leukemia. *N. Engl. J. Med.* **350**, 1617–1628 (2004).
13. Zou, H.Y. *et al.* An orally available small-molecule inhibitor of c-Met, PF-2341066, exhibits cytoreductive antitumor efficacy through antiproliferative and antiangiogenic mechanisms. *Cancer Res.* **67**, 4408–4417 (2007).
14. Mohammadi, M. *et al.* Crystal structure of an angiogenesis inhibitor bound to the FGF receptor tyrosine kinase domain. *EMBO J.* **17**, 5896–5904 (1998).
15. Sporn, M.B. & Todaro, G.J. Autocrine secretion and malignant transformation of cells. *N. Engl. J. Med.* **303**, 878–880 (1980).
16. Loriaux, M.M. *et al.* High-throughput sequence analysis of the tyrosine kinome in acute myeloid leukemia. *Blood* **111**, 4788–4796 (2008).
17. Haq, R. *et al.* Constitutive p38HOG mitogen-activated protein kinase activation induces permanent cell cycle arrest and senescence. *Cancer Res.* **62**, 5076–5082 (2002).
18. Majeti, R. *et al.* Dysregulated gene expression networks in human acute myelogenous leukemia stem cells. *Proc. Natl. Acad. Sci. USA* **106**, 3396–3401 (2009).
19. Robinson, D.R., Wu, Y.M. & Lin, S.F. The protein tyrosine kinase family of the human genome. *Oncogene* **19**, 5548–5557 (2000).
20. Zheng, R., Klang, K., Gorin, N.C. & Small, D. Lack of KIT or FMS internal tandem duplications but co-expression with ligands in AML. *Leuk. Res.* **28**, 121–126 (2004).
21. Zhou, J. *et al.* Enhanced activation of STAT pathways and overexpression of survivin confer resistance to FLT3 inhibitors and could be therapeutic targets in AML. *Blood* **113**, 4052–4062 (2009).
22. Sato, T. *et al.* FLT3 ligand impedes the efficacy of FLT3 inhibitors *in vitro* and *in vivo*. *Blood* **117**, 3286–3293 (2011).

ONLINE METHODS

Reagents. All reagents were of American Chemical Society grade and were obtained from Thermo Scientific, unless otherwise noted. SU11274 was obtained from Selleck (Houston, TX). Crizotinib and PD173074 were obtained from Pfizer. Recombinant human HGF was obtained from R&D Systems (Minneapolis, MN).

Cells. Cell lines were obtained from the DSMZ (Brunswick, Germany) and were cultured in RPMI-1640 medium supplemented with penicillin and streptomycin and 10% FBS, with the exception of DLD-1 and WI-38 cells, which were cultured in DMEM (Invitrogen). Suspension and adherent cells were maintained at a density of 500,000–1,000,000 cells per ml and 50–90% confluence, respectively, at 37 °C in a humidified 5% CO_2 atmosphere. Human $CD34^+$ cells were obtained from AllCells (Emeryville, CA).

RNAi screen. The inducible shRNA screen was performed as previously described[23]. Briefly, cells were transduced with feline endogenous virus produced using FLYRD18 cells. Cells selected to express the ecotropic retrovirus receptor were secondarily infected with a retrovirus expressing the bacterial tetracycline repressor, and single-cell clones were subsequently selected based on their inducibility with doxycycline after tertiary retroviral infection. A mixture of 5,087 barcoded shRNAs targeting 1,740 human genes was packaged into five pools, which were then used to infect doxycycline-inducible cells. Cells were infected in quadruplicate, selected by puromycin for 5 d, divided into two groups and cultured with or without doxycycline. After 3 weeks of culture, cells were harvested to collect genomic DNA, and shRNA barcode sequences were amplified, transcribed and coupled to either Cy5 (induced) or Cy3 (uninduced) fluorophores. Labeled probes from induced and uninduced samples were combined, and their abundance was measured using oligonucleotide microarrays. The averaged fluorescence intensities were subsequently filtered to exclude shRNAs with $P > 0.05$ among biological replicates (two-tailed t test), as well as genes with less than two independent shRNAs that caused depletion after shRNA induction. Filtered genes were then ranked in order of their relative depletion of AML cells, but not of nonmyeloid cell lines, to identify selectively required genes.

Cell transduction. pLKO.1 shRNA vectors targeting HGF and MET (**Supplementary Table 1**) were obtained from the RNAi Consortium (Broad Institute, Cambridge, MA). HGF cDNA was obtained from OriGene (Rockville, MD) and cloned into the pMSCV-hygro vector for cell transduction (Clontech). Vectors were packaged using 293T cells by cotransfection of pCMV-Δ8.9 and pCMV-VSVG plasmids with FuGENE (Roche). Cells were infected by spin inoculation in the presence of 8 μg/ml of polybrene (Sigma). Infected cells were selected with puromycin (2 μg/ml, Sigma) for 2–4 d before the analysis of the knockdown effects. For the knockdown rescue experiments, cells were first transduced with the pMSCV vector containing HGF cDNA, selected with hygromycin (100 μg/ml, Sigma) and subsequently transduced with shRNAs targeting HGF. For the transduction of primary mouse hematopoietic progenitors, pMSCV-PGK-EGFP (MPG) retroviral vectors containing PML-RARA, PLZF-RARA or AML1-ETO were packaged using the PLATE cell line (Cell Biolabs) using transfection with Fugene (Roche).

Cell growth and survival analysis. For cells transduced with shRNAs targeting HGF, cells were selected and maintained in the presence of 0.1 nM recombinant human HGF to control the timing of the effects of HGF knockdown, with removal of HGF from the culture medium 2 d before the analysis. Cell growth was assayed using CyQUANT NF (Invitrogen) and CellTiter-Glo (Promega) assays, as measured using fluorescence and luminescence emission with FLUOStar Omega (BMG Labtech, Offenburg, Germany). Apoptosis was measured using flow cytometry after staining with annexin V-FITC (Abcam) and TUNEL, according to manufacturer's instructions (Millipore), and using a BD FACSCalibur flow cytometer (BD Biosciences). The cell-cycle analysis was performed using ethanol-permeabilized cells that were treated with RNAse A and stained with propidium iodide (Abcam). The cell-cycle distributions were analyzed using ModFit (Verity Software). For methylcellulose colony forming assays, nonobese diabetic severe combined immunodeficient (NOD-SCID) interleukin-2 receptor γ (IL-2Rγ)-null mice (male and female) were transplanted with 1 million primary AML cells, and cells collected from the femurs of moribund mice were isolated after ammonium chloride red cell lysis. Viable AML cells were suspended in MethoCult H4535, cultured for 2 weeks and scored for colonies with ≥20 cells according to the manufacturer's instructions (StemCell Technologies).

Primary mouse hematopoietic progenitor cell assays. Bone marrow from 8- to 12-week-old C57BL/6 mice (male and female) was collected and lineage depleted using the EasySep Mouse Kit (StemCell Technologies). Cells were stimulated for 24 h in expansion stock supplemented with mouse IL-3 (10 ng/ml), stem cell factor (50 ng/ml) and 100 nM cortisol (Peprotech). Cells were transduced by spin inoculation with 4 μg/ml polybrene (Sigma), and after 48 h, GFP-positive cells were sorted using DakoCytomation MoFlo. For colony assays, 5,000–10,000 cells were seeded into 3 ml of MethoCult medium supplemented with mouse IL-3 (10 ng/ml), IL-6 (10 ng/ml), stem cell factor (50 ng/ml) and granulocyte-macrophage colony-stimulating factor (GM-CSF) (10 ng/ml), and treated with the drugs as indicated. After 7 d in culture, colonies were either analyzed or replated (5,000–10,000 cells per well).

Western analysis. Protein from whole cells was extracted using 0.15 M NaCl, 1% (v/v) NP-40, 0.1% (w/v) SDS and 50 mM Tris, pH 8.0, supplemented with ProteaseComplete (Roche) protease and Phosphatase Inhibitor Cocktail 3 (Sigma) phosphatase inhibitors. Protein concentrations were determined by using a bicinchoninic acid-copper reduction (Bio-Rad), and 30 μg aliquots were denatured in Laemmli buffer at 95 °C for 5 min, resolved using SDS-PAGE, transferred to polyvinylidene fluoride (PVDF) membrane (Pierce), blocked and probed using primary antibodies to MET (1:10,000; L41G3 and 3D7 from Cell Signaling Technology), HGF (1:2,000; H-145 from Santa Cruz) and β-actin (1:10,000; AC-40 from Sigma). Bound antibodies were chemiluminescently detected using horseradish peroxidase–conjugated secondary antibodies (1:100,000), SuperSignal West Dura reagent (Pierce) and the ImageQuant LAS 4000 (GE Healthcare) or G:BOX camera systems (Syngene), according to the manufacturer's instructions.

RT-PCR. Total RNA was harvested and reverse transcribed using the Cells-to-CT Kit (Life Technologies), and quantitative PCR analysis was performed using SYBR Green and the specific primers listed in **Supplementary Table 2** on an AB 7300 instrument, according to the manufacturer's instructions (Applied Biosystems). The observed fluorescence intensities were normalized using ROX dye as the reference standard, and the relative mRNA abundance was calculated by normalizing the observed threshold cycle values to those of glyceraldehyde 3-phosphate dehydrogenase (GAPDH), assuming amplification efficiencies of 2.

***HGF* gene analysis.** The global SNP analysis was performed using Affymetrix 250K SNP arrays, as described previously[24]. Fluorescence *in situ* hybridization was performed using the Vysis LSI D7S486 and CEP7 dual color probes (Abbott Molecular), as described previously[25]. *HGF* gene and mRNA sequencing was performed using the Sanger method (GENEWIZ) with the primers listed in **Supplementary Table 3**.

Nanoimmunoassays. Protein from whole cells was extracted using mammalian protein extraction reagent (M-PER) (Pierce) supplemented with ProteaseComplete (Roche) protease and Phosphatase Inhibitor Cocktail 3 (Sigma) phosphatase inhibitors and diluted to final concentration of 0.1 mg/ml, as measured using bicinchoninic acid-copper reduction (Bio-Rad). Aliquots of 300 ng were diluted twofold with Ampholyte pH 4-9 and resolved by capillary isoelectric focusing electrophoresis using the NanoPro 1000 instrument (Cell Biosciences). Resolved proteins were immobilized by ultraviolet crosslinking, according to the manufacturer's instructions, and probed with antibodies to the following at a 1:100 dilution for 120 min: MET (L41G3, 3D7, 25H2 and D26 from Cell Signaling Technology), HGF (H-145 from Santa Cruz and AF2207 from R&D Systems), STAT3 (9132 from Cell Signaling Technology), ERK1/2 (06182 from Millipore), CRKL (32H4 from Cell Signaling Technology), cleaved CASP3 (9661 from Cell Signaling Technology) or FGFR1 (ab823 from Abcam

doi:10.1038/nm.2819

and 55H2 from Cell Signaling Technology). Phosphorylation-specific isoforms were identified by blotting with phosphorylation-specific antibodies (D26 and 55H2 from Cell Signaling Technology for phosphorylated MET (pMET) and pFGFR1, respectively) or by using published nanoimmunoassays (Cell Biosciences). Proteins were detected by time-resolved chemiluminescence (60, 120, 240 and 960 millisecond exposures) using appropriate horseradish peroxidase–conjugated secondary antibodies and probed at a 1:100 dilution for 60 min. Time-resolved chemiluminescence profiles were used to identify the linear detection range, and those profiles in the linear detection range were fit to calculate peak areas and carry out baseline subtraction, as implemented in Compass 1.4.3 (Cell Biosciences).

Immunohistochemistry. Immunohistochemistry was performed using 4-μm formalin-fixed, paraffin-embedded tissue sections, which were soaked in xylene, passed through graded alcohols and washed in distilled water. For HGF and MET, slides were pretreated in a steam pressure cooker (decloaking chamber, BioCare Medical) with 1 mM EDTA, pH 8.0, and 10 mM citrate, pH 6.0, respectively. For HGF, antibody to human HGF (AF-294NA, R&D Systems) was applied in Dako diluent at 1:250 for 1 h. For MET, antibody to human MET (MET4, G.V.W.) was applied in Dako diluent at 1:500 for 1 h. Slides were then washed, and the appropriate secondary antibodies were applied at 1:1,500 in Dako diluent for 1 h. Immunohistochemical staining was detected using the EnVision+ kit, as per the manufacturer's instructions (Dako). Staining was quantified using the Aperio Digital Pathology Environment (Aperio). Specimens were classified as coexpressing HGF and MET if AML blasts identified by their morphology expressed 1+ (low), 2+ (moderate) or 3+ (high) of both proteins.

Primary specimens. AML diagnostic specimens were collected with informed consent and the approval of the Institutional Review Boards of the University of Manchester or the Dana-Farber Cancer Institute.

Mouse xenografts. Mouse studies were conducted with the approval of the Institutional Animal Care and Use Committee (Dana-Farber Cancer Institute and Northwestern University). NOD-SCID IL-2Rγ–null mice at 6–8 weeks of age (Jackson Laboratory) were transplanted with 1 million cells modified to express firefly luciferase by tail vein injection. Leukemia burden was monitored using whole-body bioluminescence, as previously described[26]. Mice were imaged every 5–7 d after injection, and mice with established leukemia, as assessed by exponentially increasing bioluminescence, were divided into treatment cohorts. Crizotinib and PD173074 were dissolved in aqueous 50 mM sodium acetate, pH 4 (vehicle), and were administered in combination, with at least 4 h between the administration of the individual drugs. Disease burden after treatment was assessed using serial imaging, flow cytometry and nanoimmunoassays. Peripheral blood and femoral bone marrow cells were harvested using standard methods and depleted of red cells using ammonium chloride lysis before analysis. For nanoimmunoassays, human AML cells were further purified using human-specific CD45 MicroBeads (MACS Miltenyi Biotec).

Flow cytometry. CD34-purified AML cells were fixed and permeabilized with 70% ethanol and stained with either IgG1 κ isotype control (1:10,000; eBioscience) or specific antibodies (1:10,000; MET: L41G3 and 3D7 from Cell Signaling Technology; HGF: 1:2,000; H-145 from Santa Cruz). Cells stained with primary antibodies were co-stained with rabbit IgG–specific Alexa 488 and mouse IgG–specific Alexa 647 fluorescently conjugated secondary antibodies.

Collection of patient samples. For the analysis of HGF and MET expression in bone marrow biopsies of patients with AML, patients had presented to the Department of Haematology at the Manchester Royal Infirmary, UK between 1994 and 2005. The samples used comprised residual diagnostic material and were collected with informed consent and the approval of the Institutional Review Board of the University of Manchester (LREC 01/298). Freshly obtained trephine biopsies were immediately fixed in 10% (v/v) neutral buffered formalin (Genta Medical) for 24 h and decalcified in 20% (w/v) EDTA, pH 7.4, for 48 h. Samples were dehydrated and embedded in paraffin wax using a Leica ASP300 smart tissue processor (Leica Microsystems). For the analysis of MET signaling, bone marrow aspirates were collected from patients at the Dana-Farber Cancer Institute and viably frozen in 10% DMSO after obtaining informed consent (DFCI 01-206). For nanoimmunoassays and flow cytometry analyses, cells were thawed, depleted of red cells using ammonium chloride lysis and purified using human CD34 MicroBeads (MACS Miltenyi Biotec).

Data and statistical analyses. The doubling time was calculated using the formula $t_{1/2} = i \ln 2/\ln (c_2/c_1)$, where c_2 and c_1 are the number of cells at the end and beginning of the time interval i, respectively. IC_{50} was calculated using the formula $y = a + (b - a)/(1 + x/IC_{50})^n$, where y is cell viability, a and b are the high and low baselines, respectively, x is drug concentration and n is the Hill coefficient. The combined drug effects were analyzed using the median effect method as implemented in CalcuSyn 2.0 (Biosoft). Time-to-event distributions were calculated using the Kaplan-Meier method. Statistical significance was assessed using Student's t test with two-tailed comparisons for biological measurements and using the log rank test for the comparison of survival distributions. Calculations were performed using Origin 8 (Microcal).

Additional methods. Detailed methodology is described in the **Supplementary Methods**.

23. Ngo, V.N. *et al.* A loss-of-function RNA interference screen for molecular targets in cancer. *Nature* **441**, 106–110 (2006).
24. Heinrichs, S. *et al.* Accurate detection of uniparental disomy and microdeletions by SNP array analysis in myelodysplastic syndromes with normal cytogenetics. *Leukemia* **23**, 1605–1613 (2009).
25. Mathew, P. *et al.* Detection of MYCN gene amplification in neuroblastoma by fluorescence *in situ* hybridization: a pediatric oncology group study. *Neoplasia* **3**, 105–109 (2001).
26. Armstrong, S.A. *et al.* Inhibition of FLT3 in MLL. Validation of a therapeutic target identified by gene expression based classification. *Cancer Cell* **3**, 173–183 (2003).